

Page Proof Instructions and Queries

Please respond to and approve your proof through the “Edit” tab, using this PDF to review figure and table formatting and placement. This PDF can also be downloaded for your records. We strongly encourage you to provide any edits through the “Edit” tab, should you wish to provide corrections via PDF, please see the instructions below and email this PDF to your Production Editor.

Journal Title: Journal of Applied Biomaterials & Functional Materials
Article Number: 1111875

Thank you for choosing to publish with us. This is your final opportunity to ensure your article will be accurate at publication. Please review your proof carefully and respond to the queries using the circled tools in the image below, which are available in Adobe Reader DC* by clicking **Tools** from the top menu, then clicking **Comment**.

Please use *only* the tools circled in the image, as edits via other tools/methods can be lost during file conversion. For comments, questions, or formatting requests, please use . Please do *not* use comment bubbles/sticky notes .



*If you do not see these tools, please ensure you have opened this file with **Adobe Reader DC**, available for free at get.adobe.com/reader or by going to **Help > Check for Updates** within other versions of Reader. For more detailed instructions, please see us.sagepub.com/ReaderXProofs.

No.	Query
GQ1	Please confirm that all author information, including names, affiliations, sequence, and contact details, is correct.
GQ2	Please confirm that the Funding and Conflict of Interest statements are accurate.
GQ3	Please note that we cannot add/amend ORCID iDs for any article at the proof stage. Following ORCID’s guidelines, the publisher can include only ORCID iDs that the authors have specifically validated for each manuscript prior to official acceptance for publication.
1	Please check that the correct license type appears on your article and matches what you had specified in the SAGE Open Access Portal. Please ensure that, where applicable, the responsible bill payer has paid the Article Processing Charge (APC) via the SAGE Open Access Portal for timely publication of your article.
2	Please Provide Complete Postal Address for Corresponding Author.
3	Please Confirm 8th Author Name.
4	Please check Part label captions and descriptor in Figure 3 and 8.

The fabrication of halloysite nanotube-based multicomponent hydrogel scaffolds for bone healing

Journal of Applied Biomaterials &
Functional Materials
1–15

© The Author(s) 2022

Article reuse guidelines:

sagepub.com/journals-permissions

DOI: 10.1177/22808000221111875

journals.sagepub.com/home/jbf



Saeideh Same¹, Jamileh Kadkhoda², Golnaz Navidi³,
Fatemeh Abedi⁴, Marziyeh Aghazadeh⁵, Morteza Milani⁶,
Abolfazl Akbarzadeh⁷ and Soodabeh Davaran² [GQ: 1][AQ: 3]

Abstract

Bone tissue engineering, as an alternative for common available therapeutic approaches, has been developed to focus on reconstructing of the missing tissues and restoring their functionality. In this work, three-dimensional (3D) nanocomposite scaffolds of polycaprolactone-polyethylene glycol-polycaprolactone/gelatin (PCEC/Gel) were prepared by freeze-drying method. Biocompatible nanohydroxyapatite (nHA), iron oxide nanoparticle (Fe_3O_4) and halloysite nanotube (HNT) powders were added to the polymer matrix aiming to combine the osteogenic activity of nHA or Fe_3O_4 with high mechanical strength of HNT. The scanning electron microscope (SEM) methods was utilized to characterize the nanotube morphology of HNT as well as nanoparticles of Fe_3O_4 and nHA. Prepared scaffolds were characterized via Fourier-transform infrared spectroscopy (FTIR), X-ray diffraction analysis (XRD), and SEM methods. In addition, the physical behavior of scaffolds was evaluated to explore the influence of HNT on the physicochemical properties of composites. Cell viability and attachment were investigated by MTT (3-(4,5-dimethylthiazol-2-yl)-2,5-diphenyl-2H-tetrazolium bromide) assay and SEM on human dental pulp-derived mesenchymal stem cells (h-DPSCs) in-vitro. Cell proliferation was observed without any cytotoxicity effect on h-DPSCs for all examined scaffolds. Alizarin red (ARS) and alkaline phosphatase (ALP) staining were carried out to determine the osteoconductivity of scaffolds. The data demonstrated that all PCEC/Gel/HNT hydrogel scaffolds supported osteoblast differentiation of hDPSCs with moderate effects on cell proliferation. Moreover, PCEC/Gel/HNT/nHA with proper mechanical strength showed better biological activity compared to PCEC/Gel/HNT/ Fe_3O_4 and PCEC/Gel/HNT scaffolds. Therefore, this study suggested that with proper fillers content, PCEC/Gel/HNT nanocomposite hydrogels alone or in a complex with nHA, Fe_3O_4 could be a suitable candidate for hard tissue regeneration.

Keywords

Bone regeneration, hollysite nanotube, nanohydroxyapatite, magnetic composite

Date received: 6 February 2022; revised: 25 May 2022; accepted: 14 June 2022

¹Research Center for Pharmaceutical Nanotechnology, Tabriz University of Medical Sciences, Tabriz, Iran

²Department of Medicinal Chemistry, Faculty of Pharmacy, Tabriz University of Medical Sciences, Tabriz, Iran

³Organosilicon Research Laboratory, Faculty of Chemistry, University of Tabriz, Tabriz, Iran

⁴Clinical Research Development, Unit of Tabriz Valiasr Hospital, Tabriz University of Medical Sciences, Tabriz, Iran

⁵Stem Cell Research Center and Oral Medicine Department of Dental Faculty, Tabriz University of Medical Sciences, Tabriz, Iran

⁶Faculty of Advanced Medical Science, Tabriz University of Medical Sciences, Tabriz, Iran

⁷Department of Medicinal Chemistry, Faculty of Pharmacy, Tabriz University of Medical Science, Tabriz, Iran

Corresponding author:

Soodabeh Davaran, Drug Applied Research Center, Tabriz University of Medical Science, Tabriz 51664, Iran.

Email: davaran@tbzmed.ac.ir [AQ: 2]



Creative Commons Non Commercial CC BY-NC: This article is distributed under the terms of the Creative Commons

Attribution-NonCommercial 4.0 License (<https://creativecommons.org/licenses/by-nc/4.0/>) which permits non-commercial use,

reproduction and distribution of the work without further permission provided the original work is attributed as specified on the SAGE and Open Access pages (<https://us.sagepub.com/en-us/nam/open-access-at-sage>).

Introduction

Bone damages are triggered by physical trauma, systemic bone disease, or degeneration. They are challenging problems in medical fields.¹ The necessity of overcoming several limitations of effective bone tissue repairing has resulted in emerging new approaches to bone regeneration strategy which involve the reconstruction of functional and structural features of bone through the development of scaffold.² 3D scaffolds are vital platforms for in-situ bone reconstruction. These platforms are equipped with a combination of cells, bioactive agents, and other functional components to provide the proper microenvironment for cells adhesion, proliferation, and differentiation.³ The hydrogels, with high biocompatibility and biodegradability, could mimic the natural extracellular matrix (ECM) that has been found widespread utility in tissue engineering. However, the lower physical strength of hydrogels limited their clinical application. Especially the scaffolds that are designed to be used in bone healing must have enough mechanical functionality to act as a supportive medium toward applied loads during newly forming bone tissue.^{4,5}

An increasing number of hydrogel/polymer hybrid composites were fabricated to enhance mechanical properties and osteogenic performance. The amphiphilic PCL-PEG-PCL copolymer composition with biodegradable gelatin can enhance hydrogel surface features in cell adhesion, migration, and osteogenesis.⁶

In addition, various methods and materials have been utilized to modify the bioactivity of designed scaffolds.

Nano-hydroxyapatite (nHA) bioceramic as the main substance of human bones, is the inorganic biomaterial that found wide application in the bone regeneration field. HA with structural and chemical similarity to bone minerals exhibited superior bioactivity and extended osteoconductivity.^{7,8} Calcium deficient hydroxyapatite and gelatin were utilized in the fabrication of an injectable bone filler to mimic native bone tissue for craniofacial and orthopedic regeneration.⁹

However, the addition of pure HA decreases the mechanical strength of composites which affects their utilization as a long-lasting high-load-bearing implant prosthesis. Therefore, different attempts have been made to lessen the aforementioned disadvantage.¹⁰ The TiO₂ doped chitosan/hydroxyapatite scaffold was reinforced via HNT to be applied as a template intended for directed bone tissue regeneration.¹¹

Iron oxide nanoparticles (i.e. Fe₃O₄ NPs) with great biocompatibility and exclusive magnetic properties are important components with considerable attention for hard tissue regeneration.¹² The Fe₃O₄ nanoparticle (MNP) at diameters of <20 nm can act as a single magnetic domain to provide a micromagnetic environment without applying the external magnetic force. Therefore, MNP incorporated in the polymeric bio-scaffolds could create micro-magnetic dynamic

force at the interface of scaffold and cell that activate the cell surface receptors for enhancing cell performance and improving osteogenic processes of bone formation.^{13,14}

Several studies have confirmed magnetic field impact on the stimulation of biocompatible scaffolds in terms of improving cellular-scaffold interaction and stem cells fate.¹⁵

In this context, magnetic scaffolds were designed through magnetic guiding of 3D controlled cell seeding.¹⁶ The integration of Fe₃O₄ magnetic nanoparticles in scaffolds' matrix promoted the differentiation and proliferation of BMSCs (bone mesenchymal stem cells).¹⁷ The fabricated magnetic nanocomposite scaffold acted as a potential template for autologous bone transplantation in rabbits in vivo.¹⁸ However, despite magnetic nanoparticles that were approved by the FDA (Food and Drug Administration), the supplementary oxidative stress and reactive hydroxyl radical formation throughout the reaction progression of nanoparticles and hydrogen peroxide (H₂O₂) in complex lesions limit their application in bone remodeling.¹⁹ The incorporation of Fe₃O₄ NPs with another biomaterial in scaffolds could reduce the cytotoxic effect via optimizing its needed concentration for superior biomedical activity.²⁰ The synthesized multifunctional nano scaffolds through surface modification of HNT with Fe₃O₄, calcium phosphate, and chitosan improved the osteogenesis performance of human adipose tissue-derived mesenchymal stem cells.²

Based on the aforementioned subject, there is extensive attention to the distinctive medicinal and biological features of halloysite nanotubes (HNTs) that will be significant in designing templates for clinical uses.²¹ HNT as a natural aluminosilicate (Al₂Si₂O₅ (OH)₄-2H₂O) is a specific porous nanotubular inorganic nanofillers. HNTs, as biocompatible and non-toxic materials, with appropriate mechanical strength and high surface area, have been doped in bone regeneration scaffolds to enhance mechanical strength and composite attachment to implanted bone.²² In addition, the unique structure of the inner and outer layers of hollow tubes, especially the existence of Si in the form of a silicate group on the outer layer of HNT provides a special potential for these well-crystallized kaolin clay to be effective in improving osteoblast differentiation.²³

Therefore, we assumed to modify Fe₃O₄ and nHA-PCEC/Gel scaffolds via incorporating HNT and compare their physical and biological features with each other and with pure HNT/PCEC/Gel scaffold at the same concentration, as well. Mechanical strength, morphology, and osteogenic activity of the HNTs incorporated scaffolds were studied. Prepared nHA/HNT/PCEC/Gel hydrogels exhibited the best mechanical and osteogenic activity of bone formation. This work highlights HNT bone regeneration capacity and supports the potential exploitation of all three HNT/PCEC/Gel scaffolds as a platform for the restoration of damaged bone in variable types, ages, and other health factors.

Material and method

Material

ϵ -Caprolactone, polyethylene glycol with Mw of (6000), gelatin, glutaraldehyde (25% aqueous solution), sodium hydroxide, and acetic acid were supplied from Merck Chemical Co. Nanohydroxyapatite powder (with particle size <70 nm) and Magnetite iron oxide nanoparticle (II, III) powder (mostly 20–30 nm), dichloromethane stannous octoate, and dichloromethane were supplied from Sigma-Aldrich. Halloysite (with a diameter of 30–70 nm and length of 1–3 μ m) was obtained from natural nano (Rochester, NY, USA). Fetal bovine serum (FBS), antibiotics including DMEM (Modified Eagle's Medium), penicillin streptomycin, Dulbecco, trypsin-EDTA, and PBS (phosphate buffered saline) were obtained from Gibco, Singapore. MTT powder (3-(4, 5-dimethylthiazol-2-yl)-2, 5-diphenyltetrazoliumbromide) were purchased from Invitrogen (Carlsbad, CA).

Preparation of PCEC copolymer

PCL-PEG-PCL triblock copolymer was synthesized based on the method described in previous works.²⁴ Briefly, PCI-PEG-PCL triblock was synthesized through ring-opening polymerization of ϵ -CL monomer in the presence of PEG. 1 g of PEG and 1 g of PCL monomers were mixed and melted up to 80°C in the presence of a nitrogen flow. After PEG was melted, the temperature of the mixture rose to 130°C. Octoate molten tin catalyst (0/05 wt %) was added under mild stirring and continued nitrogen gas flow. The prepared solid polymer was dissolved in dichloromethane, precipitated into icy diethyl ether, and dried at room temperature overnight.

Fabrication of PCEC/Gel based hybrid scaffold

PCEC/Gel/HNTs, PCEC/Gel/HNT/nHA, and PCEC/Gel/HNT/Fe₃O₄ were synthesized via the freeze-drying process as follows. Initially, the different types of hybrid suspensions were prepared separately in 5 ml dichloromethane following the definite amount of HNT, nHA and Fe₃O₄ specified in Table 1. Then, PCEC copolymer (100 mg) was dissolved in 10 ml dichloromethane separately. The prepared copolymer solutions were added to nanopowder suspensions and mixed thoroughly to achieve proper dispersions. After adding 1% span-80 emulsifier to the solutions of copolymer, gelatin aqueous solutions (5% w/v) were added to the dispersed solutions and homogenized (homogenizer: ULTRATURRAX, T25 Basic, Germany) at 15 mV for 6 min until the polymeric and aqueous phases mixed thoroughly. Subsequently glutaraldehyde cross-linker (1% v/v) was added dropwise under stirring for 10 min. The mixtures were then immediately injected into cooled glass Petri dishes and frozen to –20°C

Table 1. Materials percentage for preparation of porous hybrid scaffolds (a) PCEC/Gel with 3 wt% HNT, (b) PCEC/Gel with 6 wt% HNT (c) PCEC/Gel with 3 wt% HNT-3 wt% HA, and (d) PCEC/Gel with 3 wt% HNT-3 wt% Fe₃O₄.

No	Sample	HNT%*	nHA%*	Fe ₃ O ₄ %*
PCG	PCEC/Gel	–	–	–
PCGH-3	PCEC/Gel/HNT-3	3	–	–
PCGH-6	PCEC/Gel/HNT-6	6	–	–
PCGHH	PCEC/Gel/HNT/nHA	3	3	–
PCGHF	PCEC/Gel/HNT/ Fe ₃ O ₄	3	–	3

*%wt respect to polymer.

overnight. Finally, the frozen samples were lyophilized at –80°C for 48 h using a Christ freeze dryer ALPHA 1-2/LD plus to obtain porous scaffolds. To block the remaining of unreacted glutaraldehyde, scaffolds were immersed in a glycine aqueous solution (1% w/v) for 1 h at 37°C and rinsed with distilled water three times. Afterward the samples were freeze-dried again for another 24 h. All samples (0.75–1 mm height) have been prepared in triplicate.

FT-IR analysis

The chemical characterizations of the prepared PCG, PCGH-6, PCGHH, and PCGHF hybrid scaffolds were assessed by FT-IR spectroscopy (Equinox 55 LS 101, Bruker, Germany) over the wavelength range of 400–4000 cm^{–1}. The Infrared (IR) spectra of all KBr pressed samples were recorded under CO₂ nitrogen gas at room temperature.

SEM and EDX analysis

The morphology of HNT, Fe₃O₄, nHA nanoparticles were monitored by scanning electron microscope (SEM) (LEO 1430 VP, Germany). In addition, the surface morphology and structure of prepared scaffolds were visualized by SEM at 15 kV acceleration voltage. Examined Scaffolds (PCG, PCGH-6, PCGHH, and PCGHF) were sectioned into thin slices and vacuum-coated with Au–Pd thin layer by a Polaron SC7620 sputter coater. The presence and distribution of used elements on the scaffold's surface were evaluated using EDX (Energy-dispersive X-ray spectroscopy) (MIRA3TESCAN). Analyzed specimens were cut into specified sizes and placed on electron microprobe stubs.

Mechanical test

Mechanical strengths of prepared porous samples were performed at the load cell of 10N at room temperature using Zwick tensile testing machine (Germany). The scaffolds were cut into 10 mm \times 20 mm in size. For the mechanical test, compressive pressure was performed at an extension rate of 5 mm/min until the examined specimens reached to 80% reduction in height.

Porosity and density

The liquid displacement method is a reliable test to determine the porosity and density of prepared samples. Samples with a known weight (W) were immersed in a certain volume of EtOH (V_1) at a scaled cylinder. The volume of the ethanol after placing scaffolds is V_2 . The EtOH soaked scaffold was picked up and the residual volume of EtOH was recorded as V_3 . Porosity and density of examined samples were determined based on equations (1) and (2), respectively.

$$\varepsilon = \frac{(V_1 - V_3)}{V_2 - V_3} \quad (1)$$

$$\rho = \frac{W}{V_2 - V_3} \quad (2)$$

Swelling

The swelling study was performed to determine water absorption percentage. Dry with a certain weight (W_d) were immersed in phosphate buffer solution (PBS) for 24, 48, and 72 h. After immersion, the swollen samples were taken out and the excess water from their surface was removed softly by filter papers, then weighed again (W_w). The percentage of absorbed water was calculated using equilibrium (3):

$$\text{Degree of swelling (\%)} = \frac{(W_w - W_d)}{W_d \times 100} \quad (3)$$

In vitro hDPSCs cell isolation and culturing

To sterilize, composites were impregnated in ethanol (70%) for 30 min and washed with sterilized PBS three times to remove any EtOH residues. Then, they were subjected to UV spot for 20 min. Finally, scaffolds were soaked in DMEM medium and incubated for 3 days at 37°C to eliminate residual PBS.

hDPSCs were seeded in a complete medium (DMEM comprised FBS (10%), and Penicillin antibiotics (1%) and incubated at 37°C in 5% CO₂ atmosphere. As 80%–90% confluency was obtained, pre-cultured h-DPSC were detached with the mixtures of trypsin (0.05%) and 1 mM EDTA. Feasible cells were evaluated by trypan blue assay. The hDPSCs were cultured on scaffolds in a complete medium (400 ml for each well). The cell-cultured scaffolds were incubated again. TCPS contained cells without scaffolds were prepared as a control.

To evaluate differentiation performance, the osteogenic medium contained a DMEM medium with FBS (10%) and

antibiotics (1%), dexamethasone (100 nM), ascorbic acid (50 µg/ml), and β-glycerol phosphate (10 mM) was replaced by complete culture medium after 24 h. The osteogenic media was renewed every 3 days.

MTT Test for cell proliferation analysis

To evaluate the viability and proliferation of hDPSCs (passage 4) in TCPs, MTT assay was applied to PCG, PCGH-6, PCGHH, and PCGHF membrane. Cells, with a seeding density of 103 × 5 per well were cultured on pre-sterilized scaffolds for 3, 7, and 14 days. At each time point, 500 µl of MTT solution with pH=7.4 was added to each well and incubated in the dark at 37°C in 5% CO₂ atmosphere for 4 h. Then the purple-colored formazan was dissolved in 200 µl dimethyl sulfoxide (DMSO), and its optical density was determined via a microplate ELISA reader (Multiskan MK3, Thermo Electron Corporation, USA) at 570 nm. The cells seeded on TCPS were considered as a negative control. Studies were repeated in triplicate.

Cell morphology and attachment

The morphologies and adhesion of the cells cultured on scaffolds were processed and observed by SEM imaging. After 14 days, incubated scaffolds were immersed in PBS three times. Then, samples were fixed using glutaraldehyde (5%) at 37°C for 1 h, dehydrated in a series of gradient ethanol/water solutions (50%, 70%, 90%, and 100%), and air-dried at room temperature for 24 h gradient.

Alizarin red staining

ARS is a spectrophotometric determination of mineralized calcium. ARS assay was performed to assess the osteogenic activity of hDPSCs cultured on scaffolds after 21 days. The seeded scaffolds were rinsed with PBS twice and fixed with ice-cold MeOH for 1 h. Then, scaffolds were incubated in alizarin red S solution for 15 min in a dark place at room temperature. After washing with deionized water, the seeded scaffold was soaked in cetylpyridinium chloride (10% w/v) for 15 min to solubilize reacted ARS. Alizarin Red S stain concentrations were quantified via measuring the absorbance at 570 nm on the Victor3TMV reader (PerkinElmer).

Alkaline phosphatase staining

ALP activity of hDPSCs was estimated on day 21 of osteogenic induction. After washing with PBS (pH=7.4), the hDPSCs were lysed via the addition of lysis buffer (0.5 ml) containing 0.1% Triton X-10 to each well and centrifuged at 12,000 rpm for 20 min at 4°C. The supernatant from cells destruction was incubated with p-nitrophenyl phosphate solution for 30 min. The reaction was stopped by

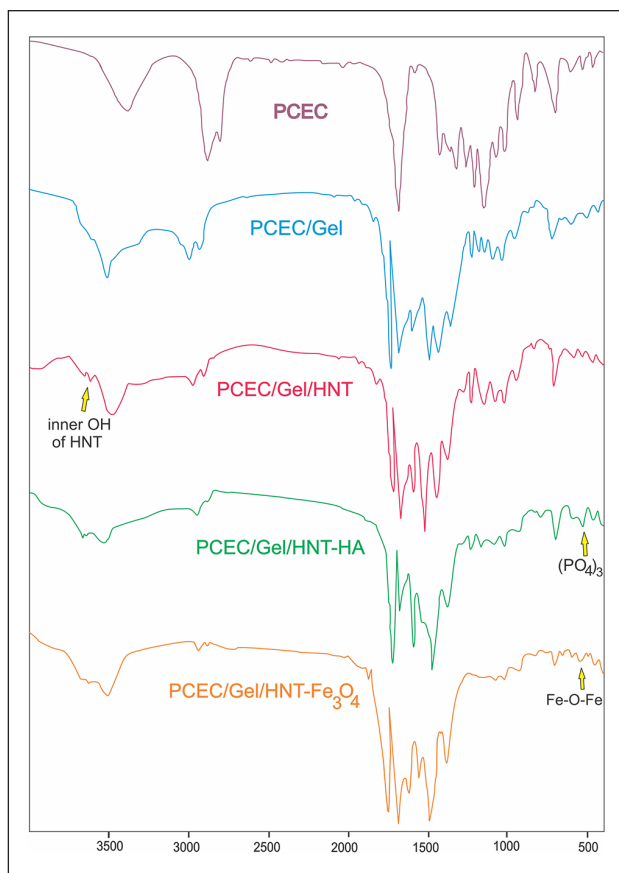


Figure 1. FT-IR spectrum of PCEC, PCEC/Gel, PCEC/Gel/HNT, PCEC/Gel/HNT/nHA, and PCEC/Gel/HNT/Fe₃O₄.

adding 600 ml of NaOH (2M). Quantification of ALP activity was controlled spectrophotometric via an automatic microplate reader at the wavelength of 405 nm.

Statistical analysis

Samples were prepared in triplicate (in size of 1 × 1 × 1 cm). All results were reported as the mean ± standard deviation (SD). The experimental data were studied using T-test and ANOVA assay. In statistical analyses, GraphPad Prism (GraphPad Software Inc, USA, version 7.03), Origin Pro (version 2022 V9.9.0.225) and $P < 0.05$ was regarded as a statistical significance level.

Results

Physical-chemical characterization

The FT-IR spectrum of different scaffolds is demonstrated in Figure 1. At the infrared spectra of PCEC copolymer, the absorption peak at 1177 and 1243 cm⁻¹ was attributed to C–O–C stretching vibration and asymmetric C–O–C stretching vibration of PEG. The C–O and C–C stretching vibration was appeared at 1368 cm⁻¹ and the peaks of C=O

stretching were shown at 1730 cm⁻¹. The absorption bands of symmetric CH₂ stretching and asymmetric CH₂ stretching were appeared at 2867 and 2948 cm⁻¹. The absorption of Terminal –OH group was shown at 3446 cm⁻¹. In the spectra of PCEC/gel, the bands appeared at 2868.60 and 2928.56 cm⁻¹ indicating the C–H stretching of PEG, PCL, and Gel. Bands at 1079.34 and 1731.89 cm⁻¹ are related to the etheric groups (C–O–C) of PEG and esteric carbonyl groups of PCL, respectively. =O stretching-hydrogen bonding joined with COO of amide-I that represented at 1638.60 cm⁻¹ and the N–H groups bending vibration and C–N groups stretching vibrations of amide-II that appeared at 1540.11 cm⁻¹ are the distinctive absorption bands of Gel. In addition, the C–N band of amide-II and III appeared at 1242.48 cm⁻¹. Bands that existed at ranges of 1463.68 to 1371.25 cm⁻¹ correspond to the methyl groups bending vibrations. The characteristic peak of N–H and COOH groups in the Gel is represented at 3441.78 cm⁻¹. As represented in the spectra of PCEC/gel/HNT, doubled bonds at 3697.07 and 3621.97 cm⁻¹ can be attributed to the stretching vibrations of the inner surface and inner hydroxyl groups of HNT, that are appeared in similar areas of PCEC/gel/HNT/nHA and PCEC/gel/HNT/Fe₃O₄ spectra. In PCEC/gel/HNT/nHA FT-IR spectrum, the peaks at 567.11 cm⁻¹ correspond to the stretching vibration of phosphate groups in nHA, where the characteristic absorption peaks of Fe–O–Fe are shown at 593.84 cm⁻¹ of PCGHF spectrum. These results confirmed that HNT, nHA, and Fe₃O₄ were immobilized in a polymeric network of the hydrogel.

The morphology of HNT, Fe₃O₄, nHA nanoparticles were provided in Figure 2. Figure 3(a)) represented the prepared PCG, PCGH-6, PCGHF and PCGHH scaffolds. In addition, the morphology and the difference among the microstructure of prepared scaffolds were visualized via SEM. As can be seen in Figure 3(b)), all the four resulting scaffolds exhibited porous morphology with interconnected pores. In addition to random dispersion, hydrogels containing nanofillers seemed to have smaller pores sizes. The EDX pattern of prepared hydrogel composites displayed in Figure 3(c)) confirmed the presence of nanofillers and their distribution on the surface of various prepared composites. The successful incorporation of different nanoparticles inside the multi-component composites were proved using EDX assay methods. The elements of Al and Si (0.24% and 0.37%) are brought by HNT of PCGH-6 that are absent in PCG (reference) diagram. Ca (0.48%) and P (0.13) are confirmed the presence of nHA in PCGHH, and 0.27% Fe belongs to Fe₃O₄ nanoparticles in PCCHF.

Mechanical analysis

The mechanical strength and stiffness of 3D scaffolds are of great importance for their promising usage in bone tissue reconstruction.²⁵ The stiffness of the membrane affects cell proliferation, adhesion, and differentiation. Since seeding

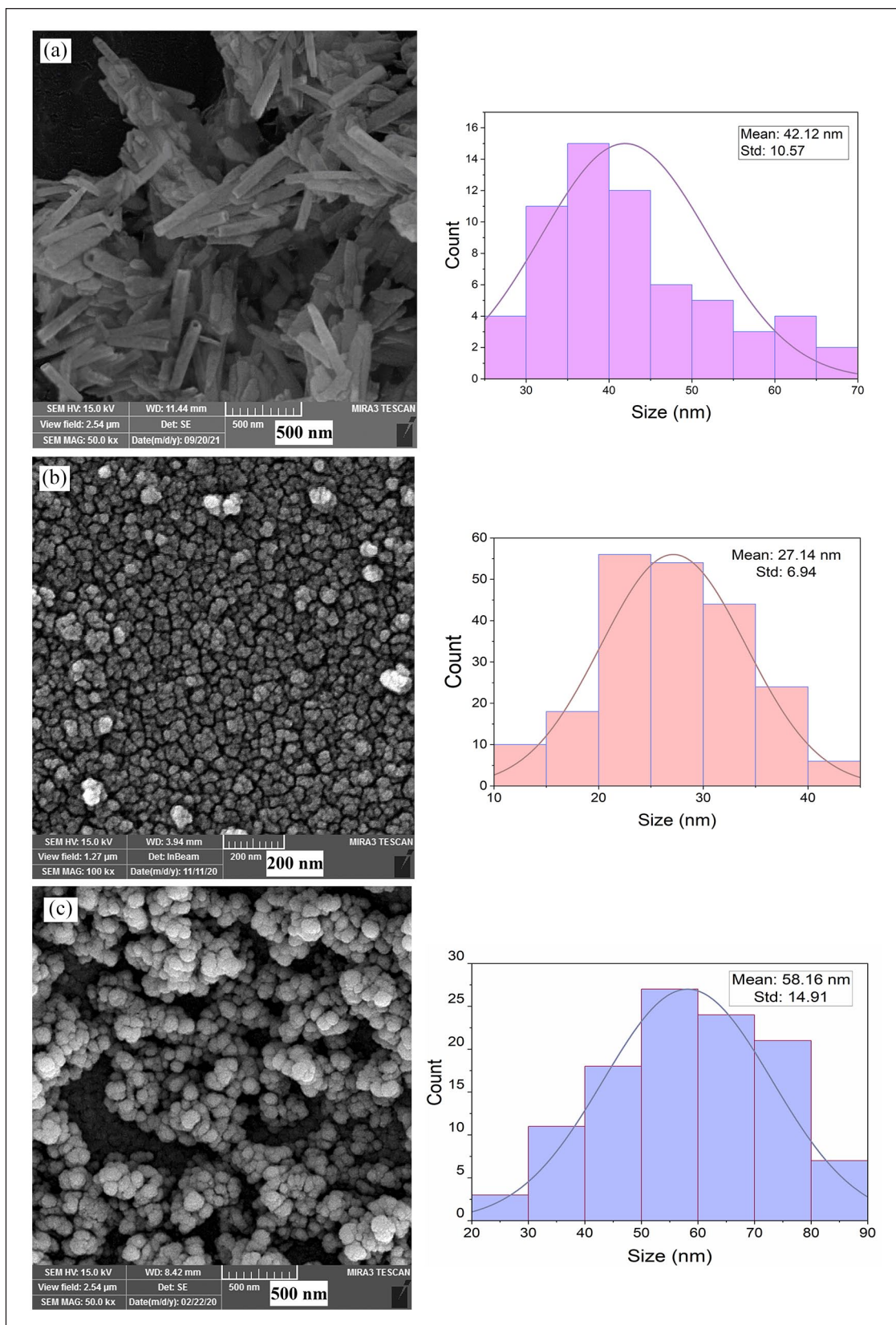


Figure 2. The SEM images of nanoparticles of (a) HNT (Scale bar: 500 nm), (b) Fe₃O₄ (scale bar: 200 nm) and (c) nHA (Scale bar: 500 nm).

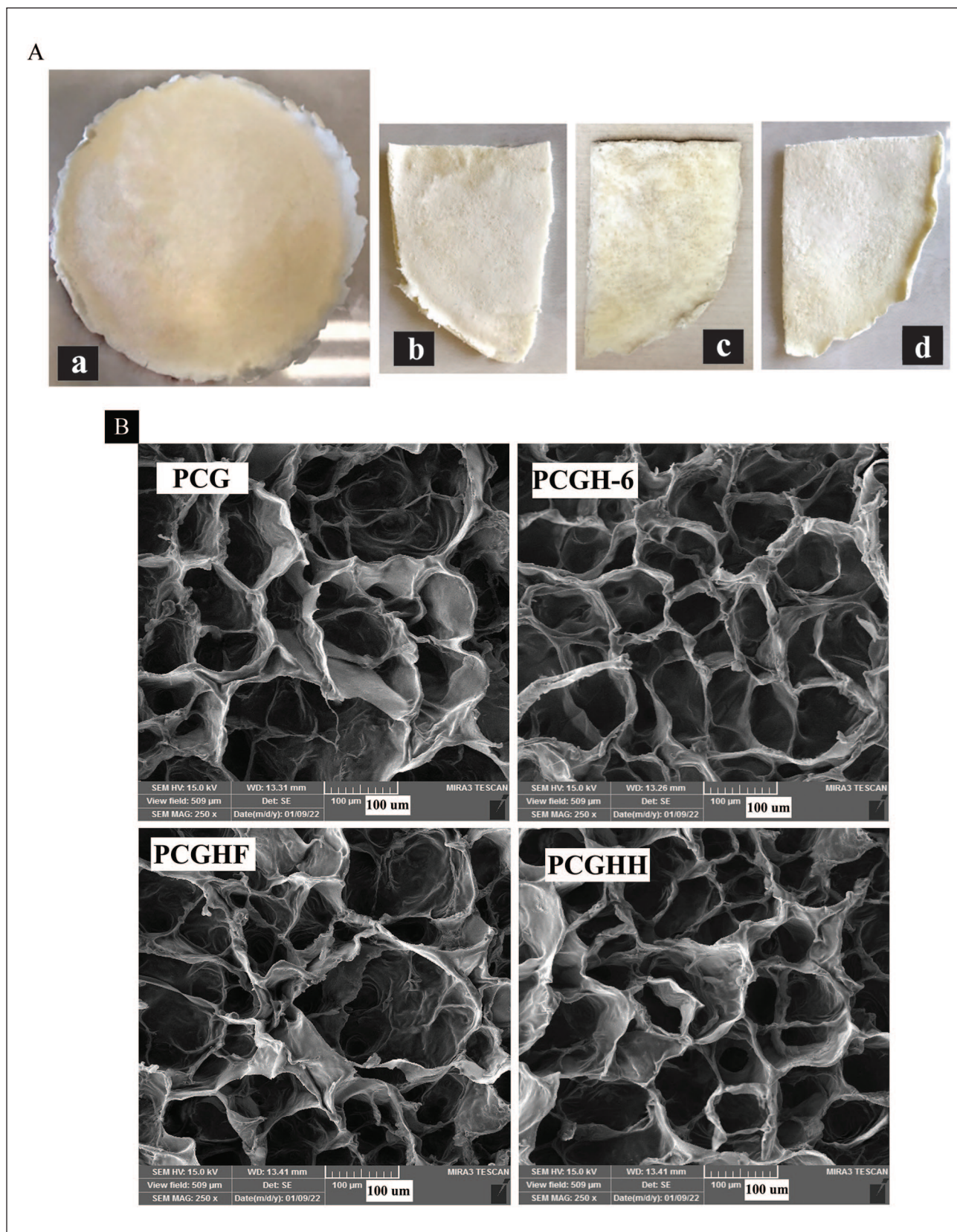


Figure 3. (Continued)

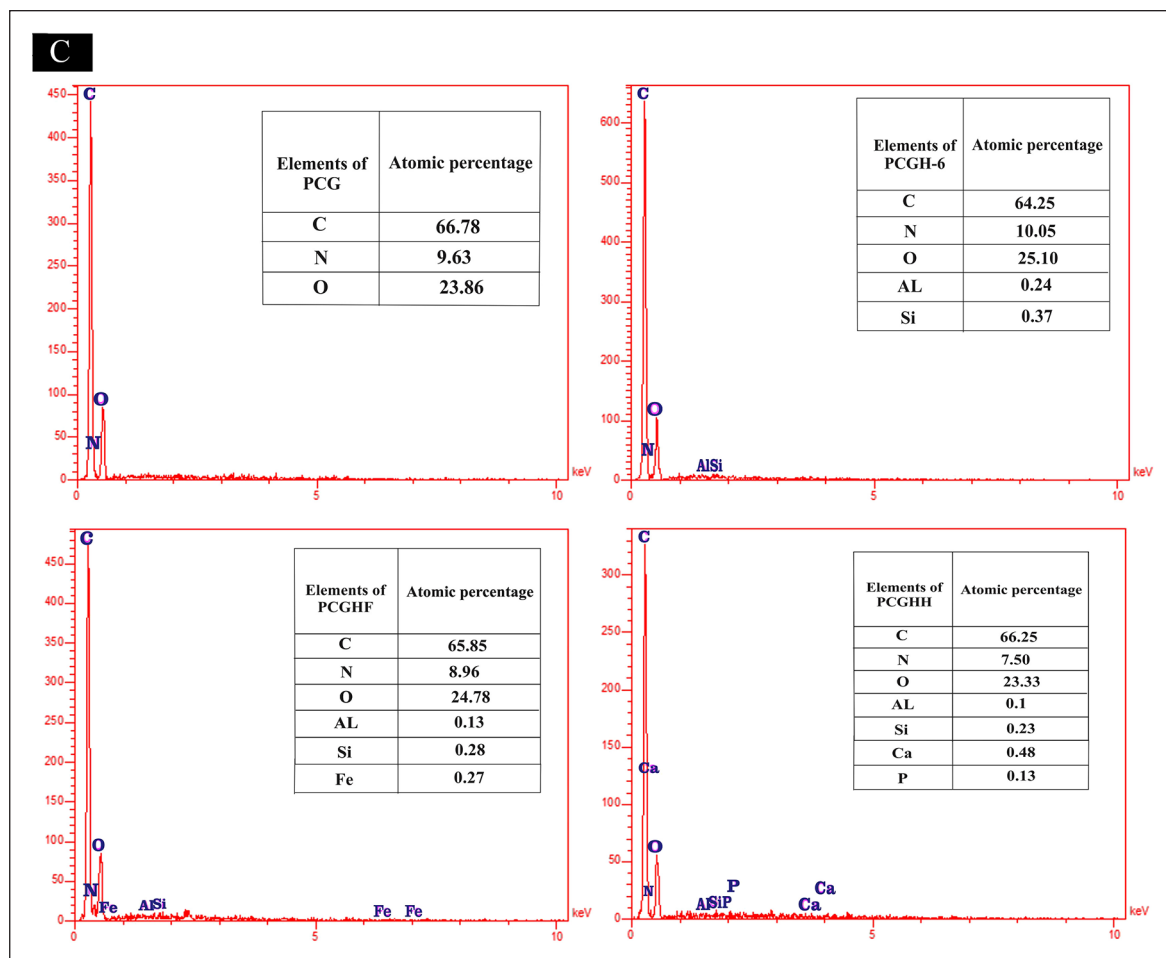


Figure 3. A. The prepared composite hydrogel scaffolds (a) PCEC/gelatin, (b) PCGH-6, (c) PCGHH and (d) PCGHF. B. The SEM images and C. EDS spectra of PCG, PCGH-6, PCGHF, and PCGHH scaffolds, (SEM scale bar: 100 μm). [AQ: 4]

cell on the scaffold with different tensile properties could adjust their interior force through the modulating of signaling pathways.²⁶ For example, research was reported that the matrix with high mechanical properties simulated MSCs to differentiate into osteoblasts while cells differentiate into nerves on the low stiffness network.²⁷ Besides, the mechanical properties of the scaffolds wrapped around the restoring bone must be of a similar magnitude to withstand physiological loading force during implantation and healing.¹² However, the implanted scaffold should keep strength at a special level to gradually degrade in a body along with the new bone generation. Of the results obtained from the stress-strain diagram in Figure 4, the stress-strain of reinforced scaffolds was improved conspicuously than the control sample (PCG composite). The mechanical properties of polymeric hydrogel containing nanofillers are higher as stiffer particles provide the rigidity for PCG scaffolds.²⁵ Especially one-dimensional HNTs with remarkable surface-to-volume ratio and tubular shape structure optimized load transmission from the PCG network to the nanotube through generating a physical network that improves its performance in bone

regeneration, as well.²⁸ It could be seen that with the inclusion of the rigid HNT particles (3% and 6% wt) to PCG hybrid hydrogel the mechanical strength was enhanced significantly. Besides, compared to the sample comprising HNT 3%, co-addition of HNT with nHA or Fe_3O_4 in PCGHH and PCGHF scaffolds showed a small reduction in scaffolds' strength (Table 2). As evident in the curves, tensile strength of PCGHF scaffolds were higher (0.93%) than PCGHH (0.91%) that revealed the superior stiffness impact of Fe_3O_4 than HA in composite scaffolds. However, increasing HNT content up to 6% wt, weakened the tensile strength of the scaffold compared to 3% slightly (from 0.96% to 0.73%), which was still higher than the control. Applying HNT in higher concentration causes non-homogeneous dispersion of HNT and aggregated particles creation in the polymer matrix which is the likely reason for lesser stiffness.²⁹

Porosity and density

Porosity and densities are important factors to examine the usefulness of scaffolds for bone tissue restoration

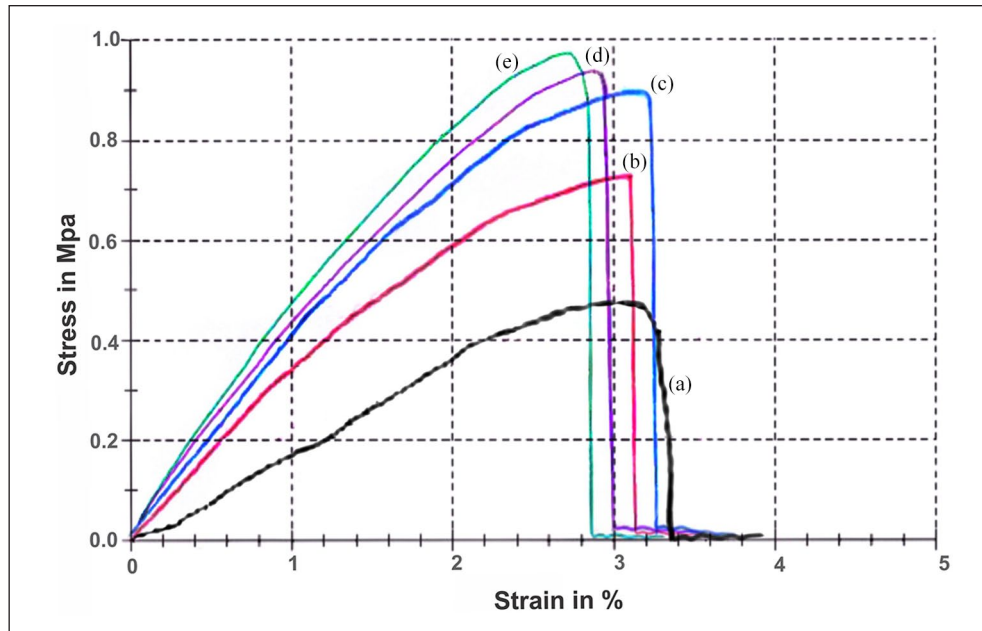


Figure 4. The stress–strain curves of (a) PCG, (b) PCGH-6, (c) PCGHH, (d) PCGHF, and (e) PCGH-3 scaffolds (with size of $1 \times 1 \times 1$ cm). Data are expressed as mean \pm standard deviation ($n=3$).

Table 2. Mechanical properties of the scaffolds.

Scaffold	Tensile strength (MPa)	Young module (MPa)
PCG	0.42 ± 0.01	0.67 ± 0.55
PCGH-3	0.96 ± 0.6	5.3 ± 0.92
PCGH-6	0.73 ± 0.29	4.7 ± 0.03
PCGHH	0.91 ± 0.11	5.3 ± 0.18
PCGHF	0.93 ± 0.74	5.1 ± 0.3

Values are mean \pm standard ($n=3$).

and cells growth.²⁸ Porosity and density should be in a balanced state for designing scaffolds with appropriate mechanical and biological features. The porous structural system with suitable pore interconnectivity facilitates ECM production, cells migration, and cell viability. Porosity supports diffusion and exchange of nutrients, oxygen, and cellular metabolites for proper osteogenesis and new tissue formation, which could be affected through the freeze-drying process.^{30,31} Besides, density is related to the pore volume and pore distribution of scaffolds. High porosity decreases the mechanical strength of scaffolds.³² Therefore, it is essential to fabricate scaffolds with great porosity and high specific surface area without reducing their strength.¹ The porosity of PCG scaffolds, created via freeze-drying, was 74.5% (Figure 5(a)). The addition of HNT with a high surface-to-volume ratio showed a stronger effect on the porosity of the scaffold that decreased the porosity, especially at 6 wt% in comparison to PCGHH or PCGHF. Previous Studies reported that halloysite nanotubes promoted the

stiffness of hydrogel scaffolds via decreasing the pore size.³³ The porosity of the nano-membranes containing HNT 3% mixed with different co-filler (Fe_3O_4 and nHA) was nearly the same, about 70% which was lower than PCG scaffold. In parallel, the density enhanced by the increasing of the nano-fillers (HNT, nHA, and Fe_3O_4) content increased (Figure 5).

Swelling

The swelling capacity of the hydrogel is vital for material exchanging during the progression of tissue reconstruction.³⁴ However, the higher degree of hydrophilicity may cause excess swelling that damages the structure and strength of the composite.³⁵ Therefore moderate swelling of the scaffolds is required for bone tissue repair.³⁶ The result of the hydrophilicity test after 24, 48, and 72 h is exhibited in Figure 5(b). As compared to PCEC/GEL composite scaffold, the addition of HNT increased the water uptake which might be related to the high surface area of applied nanotubes. However, the incorporation of Fe_3O_4 and HA decreased the water absorption capacity of scaffolds. Since the hydrophobic MNP and HA nanoparticles may form a physical barrier layer by occupying a space of porous hydrogels, which would increase the rigidity of the polymeric network and limit the water uptake of hydrophilic gelatin segments.^{37,38}

MTT assay

MTT assay was used to estimate the cell viability and cytocompatibility of prepared scaffolds toward hDPSCs.¹⁰ Figure 6 shows the OD value of seeded cells after 3, 7, and

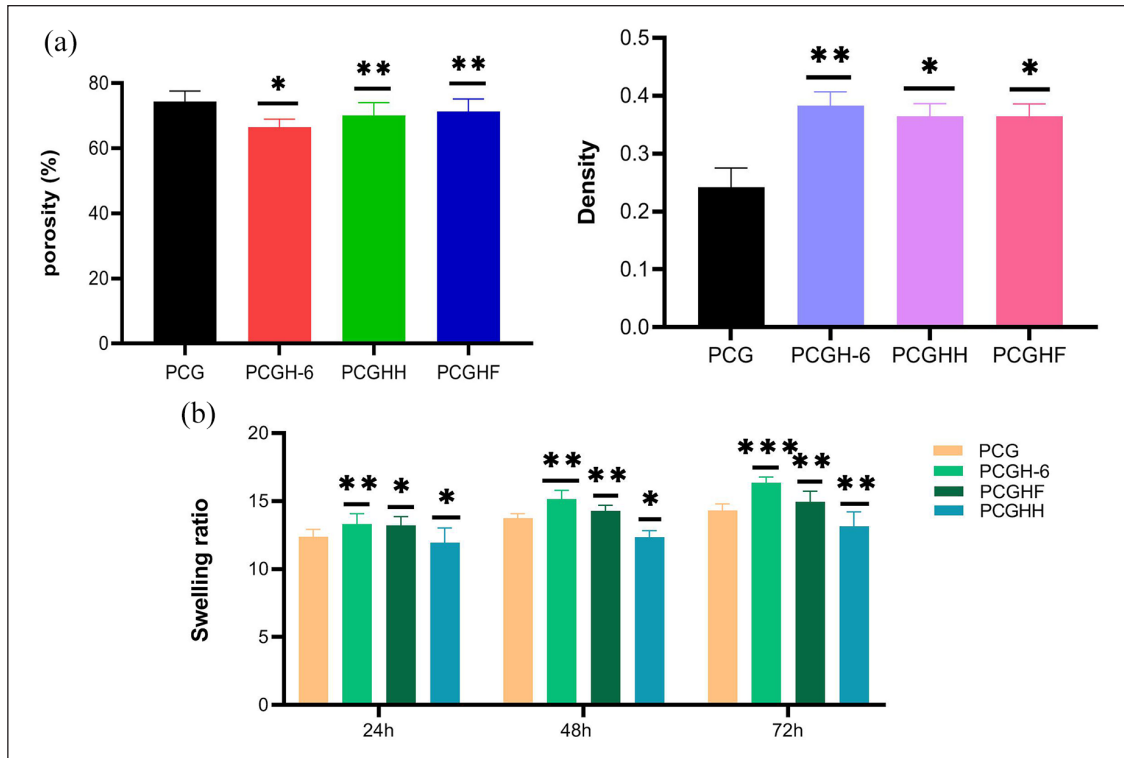


Figure 5. The porosity and density tests of the nanocomposites (a), the swelling assay in PBS at pH=7.4, 37 (b and c) (* $p < 0.05$ and ** $p < 0.01$). Data are expressed as mean \pm standard deviation ($n=3$).

14 days, in which hDPSCs were cultured on the TCPS as control. At the end of 14 days, osteoblastic cellular proliferated on all of the nano scaffolds over time. This indicates that the prepared composites are non-toxic to cultured cells. However, the cell proliferation of scaffolds containing HNT 6% decreased slightly compared to neat PCG scaffolds. In addition, it was recognized that by increasing the concentration of inorganic HNT from 3% to 6%, the growth of cells showed a little reduction. This claims that cell viability is affected by HNT concentration. Besides, by comparing the polymeric hydrogels, the addition of nHA and Fe_3O_4 improved the obtained absorbance. Remarkably, the highest cell proliferation is observed for the sample comprising nHA 3% after 3, 7, and 14 days.

Cell morphology and attachment

The morphology and in vitro adhesion of cultured cells were monitored by SEM after 14 days (Figure 7). Cells dispersed and attached randomly over the porous scaffolds confirmed the non-toxicity and biocompatibility of scaffolds. It was found that the incorporation of HNT enhanced the surface volume of scaffolds and increased their roughness relative to the pure PCG providing superior interaction between hydrogels and cells. In addition, the incorporation of magnetic Fe_3O_4 and nHA could promote cells attachment and disturb. As expected, it seems that nHA deposited composites displayed better cell adhesion and activity.

Alizarin red staining

The mineralized calcium nodules are the late-stage markers of the osteogenically differentiation process. The cell mineralization causes calcium depositions that are detailed via Alizarin red staining at their maximum concentration after 2–3 weeks of culturing.^{39,40} The extracellular calcium amount of the differentiated human-DPSCs was visualized after 21 days of seeding (Figure 8(a)). Cells cultured in nano scaffolds containing HNT, Fe_3O_4 , and nHA nanoparticles demonstrated a greater intensity of ARS activity in comparison to control (regular growth media, DMEM) and PCG scaffold, as shown in Figure 8(b). These results emphasized the positive effect of HNT support and its composition with Fe_3O_4 or nHA nanoparticles on the promotion of calcium mineralization. Growing cells on the PCGH-6 scaffolds displayed a slightly higher level of ARS activity than those on the PCGHF scaffolds. Note that the highest absorbance was detected in cells treated with PCGHH composition that proved superior osteogenesis activity of nHA immobilized-HNT scaffolds.

Alkaline phosphatase

Phosphate deposition, similar to calcium concentration, is also important for the osteogenesis of cells. Alkaline phosphatase, a membrane metalloenzyme is significant for estimating the level of mineralization and maturation of the

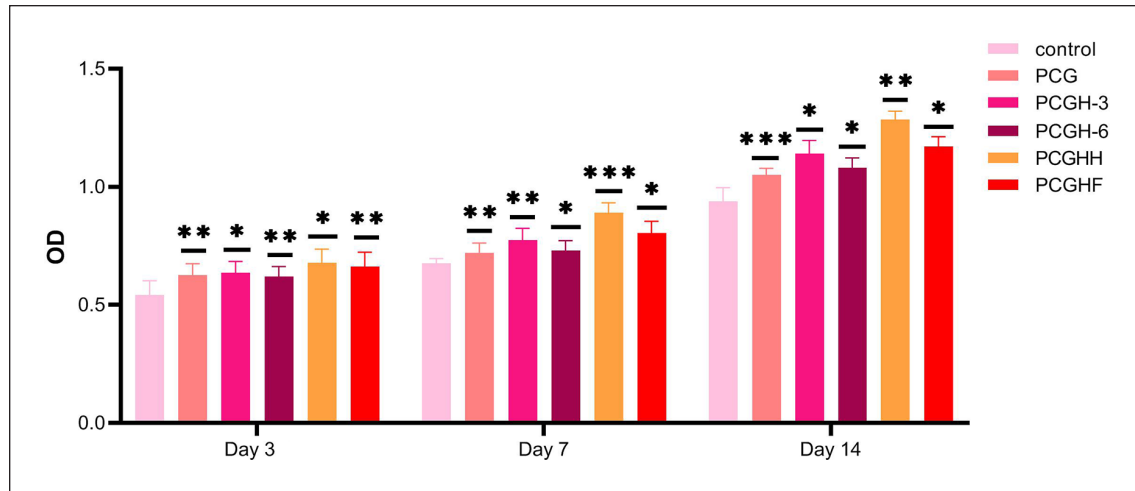


Figure 6. MTT assay of prepared scaffolds in 3, 7, and 14 days of incubation. Data are expressed as mean \pm standard deviation ($n=3$). (* $p < 0.05$, ** $p < 0.01$, and *** $p < 0.001$).

ECM during the bone regeneration progression.^{11,41} ALP activity as an osteogenic marker in the early stage of stem cell differentiation was assessed after 21 days of cell culture. According to the results depicted in Figure 8, the ALP expression of cells on the composite is higher than that on the PCG and DMEM. This higher activity can be related to the presence of HNT along with nHA and Fe_3O_4 , where ALP secretion was slightly higher in PCGH-6 in comparison to PCGHF. Furthermore, the ALP activity on scaffolds containing nHA and HNT is greatest. This confirmed the positive effects of HNT and nHA nanoparticles on enhancing the hDPSCs osteogenic differentiation.

Discussion

The present study was carried out to design biocompatible 3D scaffolds based on PCEC/Gel with the incorporation of HNT as a supportive nanofiller. The lyophilized scaffolds were examined using h-DPSCs for bone tissue engineering. The multicomponent hydrogels were prepared from PCEC/Gel and halloysite nanoclay (3%) in composition with HNT (3%), nHA (3%), or Fe_3O_4 (3%). In the fabrication of the hydrogel-based on HNT, the weight ratio of 3% was selected for HNT as an optimal value due to its superior mechanical strength and good bioactivity. Hence composite implant with poor mechanical strength could not support new bone formation in damaged sites.⁴²

In addition, materials, which are applied in scaffold preparation, have an important impact on cellular activity. So we designed three multi-component scaffolds to combine the superior mechanical strength with higher biological response in a single system, aiming to enhance cell activity and accelerate osteogenesis. Besides, as per previous reports, HNT at a concentration in a range of 5%–7% exhibited better biological activity despite its probable lower mechanical support.^{4,43} Thus, we decided to study PCGH-6 performance and

compare it with PCGHH or PCGHF composite scaffolds to examine their difference in physical strength, cellular viability, and osteoconductivity.

Mechanical studies demonstrated that PCGH-6 scaffold had lower tensile strength compared to nHA and Fe_3O_4 , which may be attributed to the agglomeration of HNT in higher concentrations. MTT assay on h-DPSCs in vitro revealed that all fabricated nanocomposites were cytocompatible with a reasonable influence on cell proliferation. Especially, the maximum cell proliferation is obtained for the sample comprising HNT/nHA where the PCGH-6 sample had slightly lower OD in comparison to PCGHH and PCGHF, as agglomerates of HNTs can affect nutrients transportation and cell growth.^{44,45} Similarly the reports revealed that the addition of HNT at high concentration (6.0 wt%) in PCL/Gel scaffold decreased cell proliferation rate without inducing cells apoptosis.^{34,46,47}

In this study, ALP and ARS staining assays were carried out after cell culturing for 21 days. Based on the results, PCGHF scaffold promoted cell osteogenic function compared to PCG scaffold. The previous work exhibited that each Fe_3O_4 nanoparticle became a single magnetism domain which promoted osteogenesis via the formation of a magnetic micro-environment, stimulating cellular signaling pathways, and reducing intracellular H_2O_2 .⁴⁸ For example, the incorporation of Fe_3O_4 MNPs in bone poly-L-lactide/polyglycolic acid scaffolds stimulated tissue formation in vivo.^{49,50} However, the studies showed that the existence of Fe_3O_4 nanoparticles in high volume ($>100 \mu\text{g}/\text{ml}$) declined cell proliferation and differentiation.⁵⁰ To overcome disadvantages, we used Fe_3O_4 nanoparticles in combination with HNT to increase mechanical and biological performance at a lower amount of Fe_3O_4 .

Interestingly, the scaffold comprising HNT 6% demonstrated higher osteogenic differentiation compared to PCGHF. It may indicate that HNT, at higher concentrations,

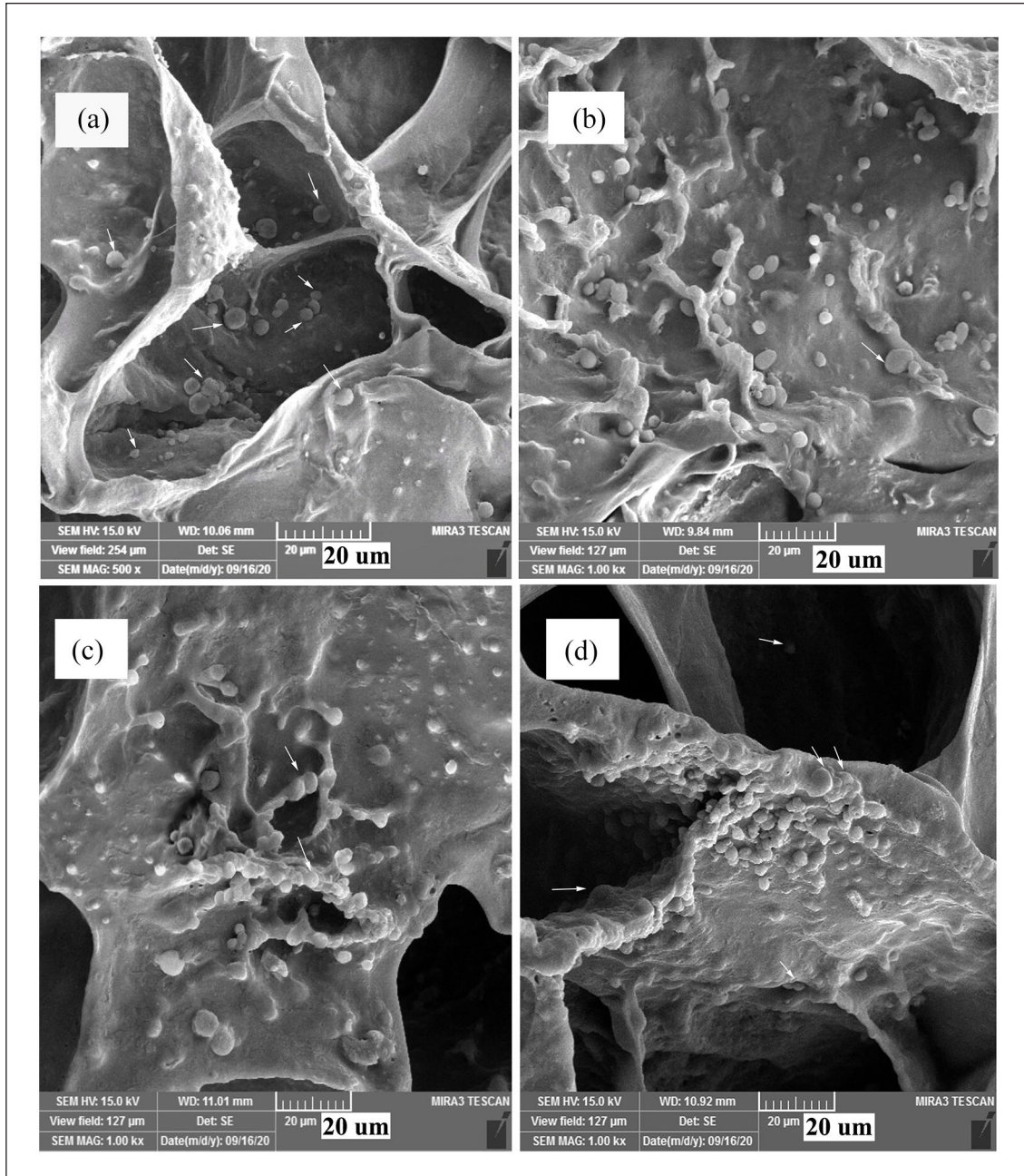


Figure 7. SEM micrographs of hDPSCs growing on (a) PCG, (b) PCGH-6, (c) PCGHF, and (d) PCGHH scaffolds (scale bar: 20 µm).

could remarkably upregulate hDPSCs osteoconductivity than being cytocompatible at lower concentrations. The existence of silica on the external surface of the halloysite increases the content of the Si element. This increment advances the bioactivity and osteoconductivity of HNT in vitro and in vivo via inducing collagen type I secretion.⁴⁷

PCGHH, with significant cytocompatibility, showed a higher promotion of osteogenic differentiation because it contains nHA ceramic, which is well known for its excellent biological activity. Chemical and structural similarity of nHA to natural bone has been reported widely in the past decade⁴⁷. However, nHA showed poor mechanical strength, especially

at the lower concentration, and it reduced applicability in long-term high-load-bearing implants.^{7,38} Nevertheless, the PCGHH scaffold displayed relatively good compressive strength due to the presence of HNT (Figure 3). In conclusion, we used HNT together with Fe_3O_4 and nHA assuming to reduce their needed volume as long as improving physical strength and maintaining or even enhancing osteogenesis. Inclusively, all three designed platforms can meet the acceptable physiological and biological performance which exhibits the possibility of applying each scaffold in bone repairing based on variability in type, age, position, or other health factors of damaged bone.

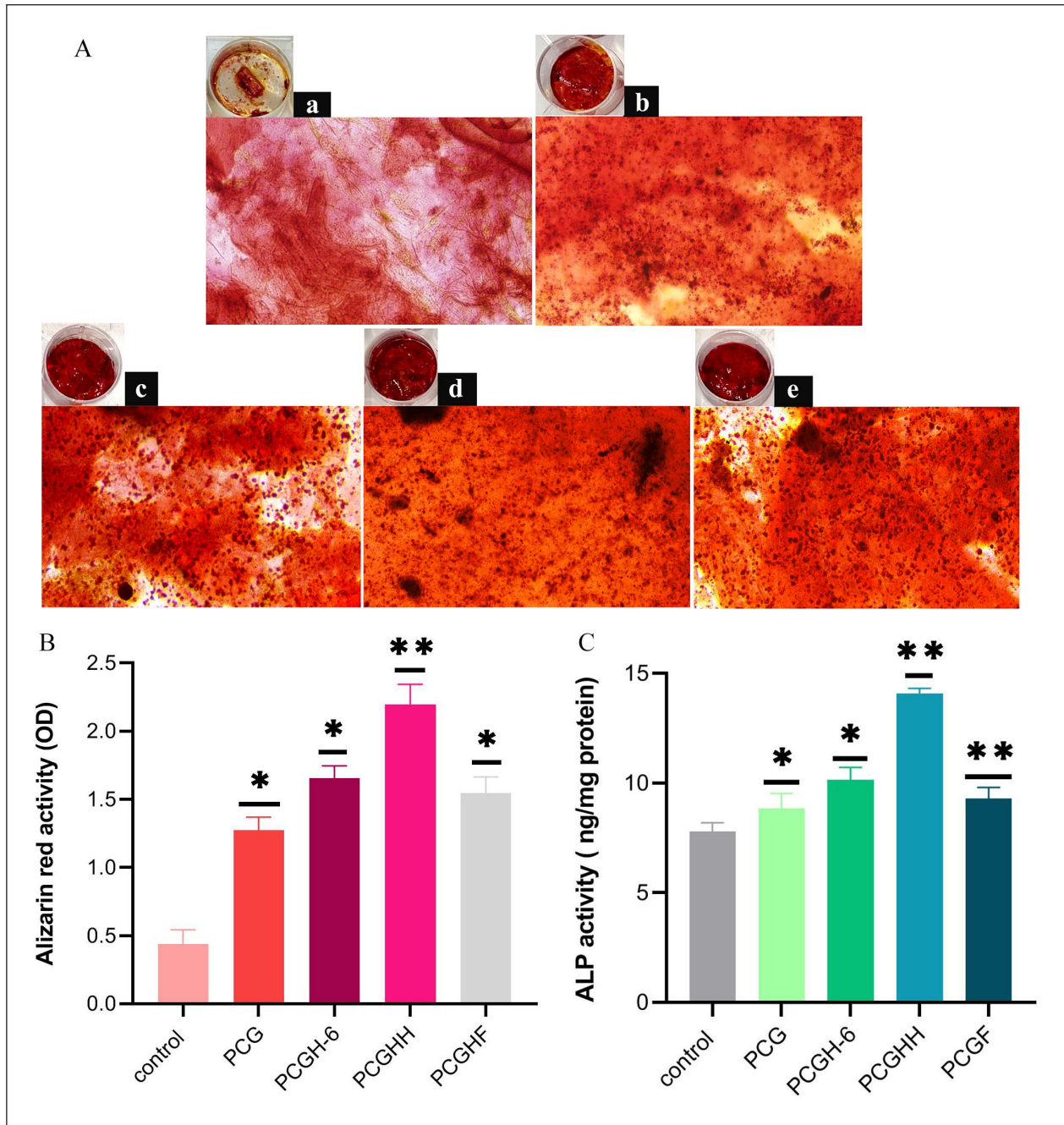


Figure 8. The photos A. of alizarin red staining for hDPSCs on the (a) control, (b) PCG, (c) PCGH-6, (d) PCGHF, and (e) PCGHH at 21 days. ARS diagram B. of calcium mineralization. Data are expressed as mean \pm standard deviation ($n=3$) (* $p < 0.05$ and ** $p < 0.01$). (Scale bar: 100 μm). C. The results of ALP activity (* $p < 0.05$ and ** $p < 0.01$).

Conclusions

3D porous scaffolds with proper physicochemical, mechanical, and biological properties are developed based on PCEC/Gel/HNT alone or in composition with HA and magnetic nanoparticles. In this work, the osteogenic activity of nHA and Fe_3O_4 were combined with the mechanical and osteogenesis performance of HNTs to design suitable potent implants for tissue regeneration. The incorporation

of HNT (3%) into PCEC/Gel scaffolds increased the mechanical performance. Freeze-dried HNT hydrogel scaffold showed supported osteoinductivity of hDPSCs in the nHA/HNT, HNT/HNT, and Fe_3O_4 /HNT scaffolds at the weight ratio of (1:1). Results indicated that newly designed PCEC/Gel/HNT scaffolds can be introduced as promising multi-component hydrogels scaffolds with superior biological and mechanical functionalities for bone tissue redevelopment.

Acknowledgements

Besides, the authors thank to the Stem Cell Research Center for guidance and help.

Declaration of conflicting interests

The author(s) declared no potential conflicts of interest with respect to the research, authorship, and/or publication of this article.

Funding [GQ: 2]

The author(s) disclosed receipt of the following financial support for the research, authorship, and/or publication of this article: This research work was funded by grant from Research Center for Pharmaceutical Nanotechnology (RCPN), Tabriz University of Medical Science (grant number 62177).

ORCID iD [GQ: 3]

Soodabeh Davaran  <https://orcid.org/0000-0002-7072-2362>

References

- Zhao W, Huang Z, Liu L, Wang W, Leng J and Liu Y. Porous bone tissue scaffold concept based on shape memory PLA/Fe₃O₄. *Compos Sci Technol* 2021; 203: 108563.
- Lee Y-J, Lee S-C, Jee SC, Sung JS and Kadam AA. Surface functionalization of halloysite nanotubes with supermagnetic iron oxide, chitosan and 2-D calcium-phosphate nanoflakes for synergistic osteoconduction enhancement of human adipose tissue-derived mesenchymal stem cells. *Colloids Surf B Biointerfaces* 2019; 173: 18–26.
- Xu HY and Gu N. Magnetic responsive scaffolds and magnetic fields in bone repair and regeneration. *Front Mater Sci* 2014; 8: 20–31.
- Huang K, Ou Q, Xie Y, et al. Halloysite nanotube based scaffold for enhanced bone regeneration. *ACS Biomater Sci Eng* 2019; 5: 4037–4047.
- Asadi N, Alizadeh E, Rahmani Del Bakhshayesh A, Mostafavi E, Akbarzadeh A and Davaran S. Fabrication and in vitro evaluation of nanocomposite hydrogel scaffolds based on gelatin/PCL–PEG–PCL for cartilage tissue engineering. *ACS Omega* 2019; 4: 449–457.
- Alipour M, Ashrafihelan J, Salehi R, et al. In vivo evaluation of biocompatibility and immune modulation potential of poly(caprolactone)–poly(ethylene glycol)–poly(caprolactone)–gelatin hydrogels enriched with nano-hydroxyapatite in the model of mouse. *J Biomater Appl* 2021; 35: 1253–1263.
- Chozhanathmisra M, Pandian K, Govindaraj D, Karthikeyan P, Mitu L and Rajavel R. Halloysite nanotube-reinforced ion-incorporated hydroxyapatite-chitosan composite coating on Ti-6Al-4V alloy for implant application. *J Chem* 2019; 2019: 1–12.
- Zhang H, Cai Q, Zhu Y and Zhu W. A simple hydrogel scaffold with injectability, adhesivity and osteogenic activity for bone regeneration. *Biomater Sci* 2021; 9: 960–972.
- Dessi M, Alvarez-Perez MA, De Santis R, Ginebra MP, Planell JA and Ambrosio L. Bioactivation of calcium deficient hydroxyapatite with foamed gelatin gel. A new injectable self-setting bone analogue. *J Mater Sci Mater Med* 2014; 25: 283–295.
- Samiei M, Aghazadeh M, Alizadeh E, et al. Osteogenic/odontogenic bioengineering with co-administration of simvastatin and hydroxyapatite on poly caprolactone based nanofibrous scaffold. *Adv Pharm Bull* 2016; 6: 353–365.
- Khan S, Kumar V, Roy P and Kundu PP. TiO₂ doped chitosan/hydroxyapatite/halloysite nanotube membranes with enhanced mechanical properties and osteoblast-like cell response for application in bone tissue engineering. *RSC Adv* 2019; 9: 39768–39779.
- Bin S, Wang A, Guo W, Yu L and Feng P. Micro magnetic field produced by Fe₃O₄ nanoparticles in bone scaffold for enhancing cellular activity. *Polymers* 2020; 12: 2045.
- De Santis R, Papallo I, Onofrio I, et al. Analyzing the role of magnetic features in additive manufactured scaffolds for enhanced bone tissue regeneration. *Macromolecular Symposia* 2021; 396: 2000314.
- Sciaila S, Barca A, Palazzo B, et al. Bioactive chitosan-based scaffolds with improved properties induced by dextran-grafted nano-maghemite and l-arginine amino acid. *J Biomed Mater Res A* 2019; 107: 1244–1252.
- Peluso V, Rinaldi L, Russo T, et al. Impact of magnetic stimulation on periodontal ligament stem cells. *Int J Mol Sci* 2021; 23: 188.
- Goranov V, Shelyakova T, De Santis R, et al. 3D patterning of cells in magnetic scaffolds for tissue engineering. *Sci Rep* 2020; 10: 2289–2298.
- Huang J, Liang Y, Jia Z, et al. Development of magnetic nanocomposite hydrogel with potential cartilage tissue engineering. *ACS Omega* 2018; 3: 6182–6189.
- Russo T, Peluso V, Fucile P, De Santis R and Gloria A. Magnetism in dentistry: review and future perspectives. *Appl Sci* 2021; 12: 95.
- Zhang H, Li S, Liu Y, et al. Fe₃O₄@GO magnetic nanocomposites protect mesenchymal stem cells and promote osteogenic differentiation of rat bone marrow mesenchymal stem cells. *Biomater Sci* 2020; 8: 5984–5993.
- Lin J, Zhang Y, Lu X, et al. Enhanced proliferation and accelerated adipogenic differentiation of mesenchymal stem cells via Fe₃O₄: insulin conjugates stimulation. *Curr Adv Cell Stem Cell* 2017; 1: 101011.
- Guo W, Xu L, Feng P, Gu Y and Shuai C. In-situ growth of silica nano-protrusions on halloysite nanotubes for interfacial reinforcement in polymer/halloysite scaffolds. *Appl Surf Sci* 2020; 513: 145772.
- Alam F, Verma P, Mohammad W, Teo J, Varadarajan KM and Kumar S. Architected poly(lactic acid)/poly(ε-caprolactone)/halloysite nanotube composite scaffolds enabled by 3D printing for biomedical applications. *J Mater Sci* 2021; 56: 14070–14083.
- Abdollahi Boraei SB, Nourmohammadi J, Sadat Mahdavi F, et al. Effect of SrR delivery in the biomarkers of bone regeneration during the in vitro degradation of HNT/GN coatings prepared by EPD. *Colloids Surf B Biointerfaces* 2020; 190: 110944.
- Saghebasl S, Davaran S, Rahbarghazi R, Montaseri A, Salehi R and Ramazani A. Synthesis and in vitro evaluation of thermosensitive hydrogel scaffolds based on (pnipaaM-PCL-PEG-PCL-pnippaaM)/Gelatin and (PCL-PEG-PCL)/Gelatin

- for use in cartilage tissue engineering. *J Biomater Sci Polym Ed* 2018; 29: 1185–1206.
25. Hokmabad VR, Davaran S, Aghazadeh M, Alizadeh E, Salehi R and Ramazani A. A comparison of the effects of silica and hydroxyapatite nanoparticles on poly(ϵ -caprolactone)-poly(ethylene glycol)-poly(ϵ -caprolactone)/chitosan nanofibrous scaffolds for bone tissue engineering. *Tissue Eng Regen Med* 2018; 15: 735–750.
 26. Jiang P, Zhang Y, Zhu C, Zhang W, Mao Z and Gao C. Fe_3O_4 /BSA particles induce osteogenic differentiation of mesenchymal stem cells under static magnetic field. *Acta Biomater* 2016; 46: 141–150.
 27. Li S, Wei C and Lv Y. Preparation and application of magnetic responsive materials in bone tissue engineering. *Curr Stem Cell Res Ther* 2020; 15: 428–440.
 28. Torres E, Fombuena V, Vallés-Lluch A and Ellingham T. Improvement of mechanical and biological properties of polycaprolactone loaded with hydroxyapatite and halloysite nanotubes. *Mater Sci Eng C* 2017; 75: 418–424.
 29. Kim J-W, Shin K-H, Koh Y-H, Hah MJ, Moon J and Kim HE. Production of poly(ϵ -caprolactone)/hydroxyapatite composite scaffolds with a tailored macro/micro-porous structure, high mechanical properties, and excellent bioactivity. *Materials* 2017; 10: 1123.
 30. Cámara-Torres M, Duarte S, Sinha R, et al. 3D additive manufactured composite scaffolds with antibiotic-loaded lamellar fillers for bone infection prevention and tissue regeneration. *Bioact Mater* 2021; 6: 1073–1082.
 31. Humayun A, Luo Y and Mills DK. Electrophoretic deposition of gentamicin-loaded ZnHNTs-Chitosan on titanium. *Coatings* 2020; 10: 944.
 32. Pazarçeviren E, Erdemli Ö, Keskin D and Tezcaner A. Clinoptilolite/PCL-PEG-PCL composite scaffolds for bone tissue engineering applications. *J Biomater Appl* 2017; 31: 1148–1168.
 33. Luo Y. *Application of halloysite nanotubes in bone disease remediation and bone regeneration*. PhD Thesis, Louisiana Tech University, USA, 2019.
 34. Chen X, Fan M, Tan H, et al. Magnetic and self-healing chitosan-alginate hydrogel encapsulated gelatin microspheres via covalent cross-linking for drug delivery. *Mater Sci Eng C* 2019; 101: 619–629.
 35. Hokmabad VR, Davaran S, Aghazadeh M, Rahbarghazi R, Salehi R and Ramazani A. Fabrication and characterization of novel ethyl cellulose-grafted-poly (ϵ -caprolactone)/alginate nanofibrous/macroporous scaffolds incorporated with nano-hydroxyapatite for bone tissue engineering. *J Biomater Appl* 2019; 33: 1128–1144.
 36. Narayanan V, Sumathi S and Narayanasamy ANR. Tricomponent composite containing copper-hydroxyapatite/chitosan/polyvinyl pyrrolidone for bone tissue engineering. *J Biomed Mater Res A* 2020; 108: 1867–1880.
 37. Amini-Fazl MS, Mohammadi R and Kheiri K. 5-Fluorouracil loaded chitosan/polyacrylic acid/ Fe_3O_4 magnetic nanocomposite hydrogel as a potential anticancer drug delivery system. *Int J Biol Macromol* 2019; 132: 506–513.
 38. Sadeghinia A, Soltani S, Aghazadeh M, Khalilifard J and Davaran S. Design and fabrication of clinoptilolite-nanohydroxyapatite/chitosan-gelatin composite scaffold and evaluation of its effects on bone tissue engineering. *J Biomed Mater Res A* 2020; 108: 221–233.
 39. Liang H, Xu X, Feng X, et al. Gold nanoparticles-loaded hydroxyapatite composites guide osteogenic differentiation of human mesenchymal stem cells through Wnt/ β -catenin signaling pathway. *Int J Nanomedicine* 2019; 14: 6151–6163.
 40. Zheng J, Wu F, Li H and Liu M. Preparation of bioactive hydroxyapatite@halloysite and its effect on MC3T3-E1 osteogenic differentiation of chitosan film. *Mater Sci Eng C* 2019; 105: 110072.
 41. Boda SK, Thirivikraman G and Basu B. Magnetic field assisted stem cell differentiation: role of substrate magnetization in osteogenesis. *J Mater Chem B* 2015; 3: 3150–3168.
 42. Ou Q, Huang K, Fu C, et al. Nanosilver-incorporated halloysite nanotubes/gelatin methacrylate hybrid hydrogel with osteoimmunomodulatory and antibacterial activity for bone regeneration. *Chem Eng J* 2020; 382: 123019.
 43. Pavliňáková V, Fohlerová Z, Pavliňák D, Khunová V and Vojtová L. Effect of halloysite nanotube structure on physical, chemical, structural and biological properties of elastic polycaprolactone/gelatin nanofibers for wound healing applications. *Mater Sci Eng C* 2018; 91: 94–102.
 44. Pazarçeviren AE, Evis Z, Keskin D and Tezcaner A. Resorbable PCEC/gelatin-bismuth doped bioglass-graphene oxide bilayer membranes for guided bone regeneration. *Biomed Mater* 2019; 14: 035018.
 45. Xue J, Niu Y, Gong M, et al. Electrospun microfiber membranes embedded with drug-loaded clay nanotubes for sustained antimicrobial protection. *ACS Nano* 2015; 9: 1600–1612.
 46. Švachová V, Khunová V, Pavliňák D, Fohlerová Z and Vojtová L. The effect of halloysite on structure and properties of polycaprolactone/gelatin nanofibers. *Polym Eng Sci* 2017; 57: 506–512.
 47. Jing X, Mi HY and Turng L-S. Comparison between PCL/hydroxyapatite (HA) and PCL/halloysite nanotube (HNT) composite scaffolds prepared by co-extrusion and gas foaming. *Mater Sci Eng C* 2017; 72: 53–61.
 48. Huang Z, He Y, Chang X, et al. A magnetic iron oxide/polydopamine coating can improve osteogenesis of 3D-printed porous titanium scaffolds with a static magnetic field by upregulating the TGF β -Smads Pathway. *Adv Healthc Mater* 2020; 9: 2000318.
 49. Shuai C, Yang W, He C, et al. A magnetic micro-environment in scaffolds for stimulating bone regeneration. *Mater Des* 2020; 185: 108275.
 50. Wu D, Chang X, Tian J, et al. Bone mesenchymal stem cells stimulation by magnetic nanoparticles and a static magnetic field: release of exosomal miR-1260a improves osteogenesis and angiogenesis. *J Nanobiotechnol* 2021; 19: 1–19.